

Efficiency Improvement of Electrospun TiO₂ Nanofibers Based Double Heterojunction Organic Photovoltaic Devices by ZnO Cathode Buffer Layer

¹ Muhammad Tanveer*, ¹ Amir Habib and ² Muhammad Bilal Khan

¹*School of Chemical and Materials Engineering, National University of Sciences and Technology, Islamabad 44000, Pakistan.*

²*Centre for Energy Systems, National University of Sciences and Technology, Islamabad 44000, Pakistan.*

mtanveerp@gmail.com*

(Received on 12th February 2013, accepted in revised form 30th May 2013)

Summary: Polymer/fullerene solar cells with cathode buffer layer and double heterojunction electrospun metal oxide nanofibers are presented in this study. Electrospun TiO₂ nanofibers on solution processed ZnO cathode buffer layer (CBL) are synthesized and introduced to inverted organic photovoltaic devices for improving their power conversion efficiency. It is found that a combination of ZnO (CBL) with electrospun TiO₂ nanofibers covers a large wavelength range for light absorption and reduced device series resistance, which improved current density and fill factor of the devices. The structural and optical properties of the various structure/ layers are investigated by FESEM and UV-Vis spectrophotometer, while the devices were characterized under 1.5G illuminations by solar simulator. The resultant efficient inverted solar cells exhibit an open circuit voltage of 0.62V, short circuit current density of 12.98mA/cm², fill factor of 0.53, and power conversion efficiency of 4.27±0.01%.

Key words: Inverted; nanofiber; buffer layer; photovoltaic

Introduction

Solar energy has the potential to meet the global growing needs for energy by providing clean, sustainable alternative to fossil fuels [1]. Organic photovoltaic (OPV) devices are much feasible for conversion of solar energy into electricity due to their low cost [2], flexible structure [3, 4], large scale [5], easiest and most versatile fabrication techniques [6-11].

The challenges regarding OPV are their comparatively low power conversion efficiency (PCE) and stability/lifetime. The performance has reasonably improved since the concept of bulk heterojunction (BHJ). There are various reports claiming high PCE relative to the controlling device, despite these efforts OPV have primary stability concern for stepping into the global market. The typical BHJ organic solar cell has a indium doped tin oxide (ITO) anode, a thin layer of poly(3,4-ethylenedioxythiophene):poly(styrenesulfonate) (PEDOT:PSS), -BHJ active layer of a blend comprising of poly(3-hexylthiophene) (P3HT) and [6,6]-phenyl C61-butyric acid methyl ester (PCBM) and a low work-function metal cathode. The structure of the OPV devices has used in an inverted configuration to overcome the challenges of stability; however the efficiency of such devices is not much higher due to low mobility of the polymer. The problem is anyhow minimized by the introduction of metal oxides in OPV devices.

The ZnO nanostructure are most widely used metal oxides because of their higher energy bandgap (3.2~3.4eV) [12-15] and carrier mobility ($4 \times 10^{-3} \text{cm}^2 \text{V}^{-1} \text{s}^{-1}$) [16]. The TiO₂/TiO_x structures are being studied both in inverted [17-19] and normal [20, 21] geometry devices. The bandgap of TiO₂/TiO_x (3.7eV) [20] is smaller than ZnO, therefore, not much favorable for use as a cathode buffer layer (CBL) in inverted structure. However, the high mobility ($10^{-6} \sim 10^{-7} \text{cm}^2 \text{V}^{-1} \text{s}^{-1}$) [22] and excellent transport properties of TiO₂ make it ideal for OPV devices to improve their performance.

There are various reports where metal oxide structures are applied to photovoltaic (PV) devices. These structures are nanodots [23], quantum dots [24], nanoparticles [17], nanorods [25-27], nanotubes [28, 29], nanowires [30] and nanofibers [31].

The nanostructures are synthesized by various techniques, the most common are sol-gel [12, 17], hydrothermal [30, 32], anodization [33], atomic layer deposition [29], and electrospinning [34]. The electrospinning technique is extensively suited for solar cell applications due to their small diameter, continuous length covering a large surface area of the substrate and most importantly controlled layer thickness. Such advantages make electrospinning the suitable nanostructure synthesizing technique for PV devices.

*To whom all correspondence should be addressed.

The light harvesting and charge collection efficiency within blended heterojunction devices are two challenges regarding the thickness of the active layer. Thick active layer harvest maximum light and result high carriers, however, on the other hand most of the carriers are lost due to poor carrier collection efficiency. There is always a tradeoff between light harvesting and maximum carrier collection efficiency by optimum active layer thickness. The other alternative of such a challenge is the introduction of nanostructure metallic oxide to enhance light harvesting and increased carrier collection. The best choices are the metal oxide porous nano structures like nanotubes having pores of the order of exciton diffusion length (5-10nm) [35-37]. Conversely, the infiltration and crystallization of polymer in small pores are a challenge. These challenges are overcome by the introduction of electrospun nanofibers. We have already demonstrated the infiltration of polymer through electrospun nanofibrous network [31]. The porous area within the nanofibrous network can be controlled by electrospinning time. TiO₂ nanotubes were used to improve the PCE of the OPV devices by double heterojunction [28]. The vertically aligned nanotubes have the disadvantage of low parallel device resistance by short to the top contact. Electrospun nanofibers based devices have high parallel resistance and therefore, increased PCE.

A high-efficiency inverted solar cell can be fabricated by utilizing a highly transparent cathode interface layer on ITO to restrain the charge recombination and enhance electron extraction. The matching of energy levels of the charge transport states in the donor material and the electrode Fermi level is important for efficient solar devices. The other critical issue regarding device performance is the energy level alignment of organic/semiconducting organic heterointerfaces, which affect both the charge separation and the open circuit voltage. The introduction of buffer layer matches/aligns the energy levels to improve the performance of the OPV devices. The reported materials for buffer layer are CdS [38], tris(8-hydroxyquinolino) aluminum (Alq3) [39], MoO₃ [15], Ca [40]. N-type metal oxide such as TiO₂ and ZnO are promising candidates due to their relatively high electron mobility, environmental stability, and high transparency. ZnO cathode layer was introduced to improve the PCE of the inverted devices [16, 19, 41, 42]. TiO_x/TiO₂ has also been studied as a cathode buffer layer in various inverted OPV devices [43-46].

In this study, we synthesized electrospun ZnO and TiO₂ nanofibers, then studied their optical properties and finally fabricated double

heterojunction devices by applying these fibers on ZnO and TiO₂ solution processed cathode buffer layer (CBL) for investigating the inverted OPV device parameters. The fabricated devices were investigated by incident photon to current conversion efficiency (IPCE) and J-V characteristics under 1.5G solar illuminations.

Results and Discussion

Fig. 1 shows the FESEM image of the TiO₂ electrospun nanofibers network. The diameter of the calcined nanofibers was 81±17nm. The cross sectional view of the TiO₂ nanofibers on ZnO CBL, the schematic and cross-sectional prior to electrode deposition of the most efficient device is shown in Fig. 2a-b.

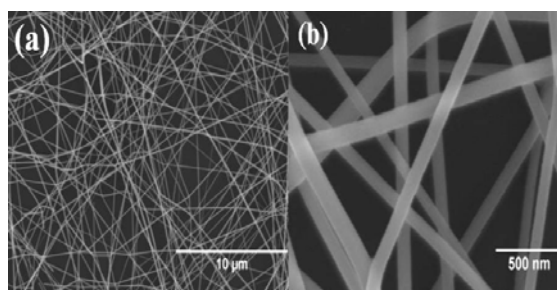


Fig. 1 FESEM of electrospun TiO₂ nanofibers calcined at 350°C for 3h; a) and b) showing continuity and porosity of nanofibers network.

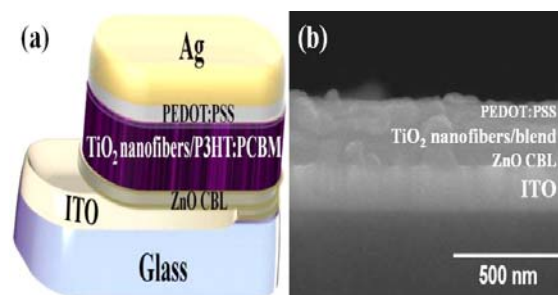


Fig. 2 Cross-sectional FESEM image and schematic of the double heterojunction organic photovoltaic devices; a) schematic of the fabricated ITO/ZnO (CBL)/electrospun TiO₂ nanofibers/P3HT:PCBM/PEDOT:PSS/Ag double heterojunction inverted organic photovoltaic device and; b) cross-sectional view of ITO/ZnO (CBL)/electrospun TiO₂ nanofibers/P3HT:PCBM/PEDOT:PSS layers prior to electrode deposition.

The ZnO electrospun nanofibers have no effect in visible range of the spectrum as indicated in

Fig. 3. The TiO₂ nanofibers have small energy bandgap compared to ZnO nanofibers therefore, showing higher absorption in the long wavelength region. The absorption shift for TiO₂ nanofibers electrospun on ZnO thin CBL attributed to the defects introduced at the interface. The absorption intensity of the P3HT:PCBM blend infiltrated in ZnO (CBL)/TiO₂ nanofibers has increased compared to the blend infiltrated in ZnO (CBL)/ZnO electrospun nanofibers and TiO₂ (CBL)/TiO₂ electrospun nanofibers, which is appreciated for solar cell devices.

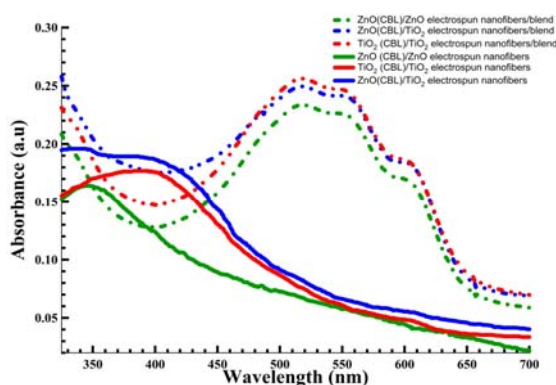


Fig. 3 UV-Vis absorption spectroscopy of electrospun nanofibers and various layers used for fabrication of inverted double heterojunction organic photovoltaic devices.

Fig. 4 shows the illuminated *J-V* characteristics of the fabricated devices under an intensity of 100mW/cm², 1.5G solar simulator. The detail of various parameters of these devices is listed in Table-1. *V*_{oc} of the devices fabricated by ZnO (CBL)/electrospun TiO₂ nanofibers was improved (0.62V) compared to the devices fabricated by using both the identical metal oxide CBL and electrospun nanofibers. This is due to a range of Fermi level for two different metal oxides. The increase in *V*_{oc} could also be attributed to band bending by ZnO (CBL)/electrospun TiO₂ nanofibers [47].

The role of double heterojunction provided by electrospun metal oxide can be investigated by improved *J*_{sc} of these devices as listed in Table-1. The increased charge collection efficiency along with high carrier mobility of these fibers has improved the *J*_{sc} of the devices. The devices fabricated by TiO₂

nanofibers have higher *J*_{sc} compared to devices fabricated by ZnO nanofibers, such effect can be attributed to the contribution of the increased carrier by higher light absorption due to the small band gap of TiO₂.

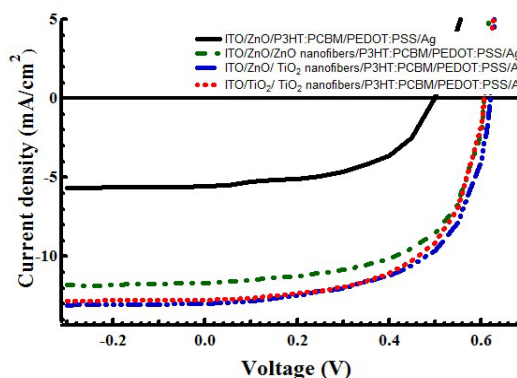


Fig. 4: *J-V* characteristics of the inverted double heterojunction OPV devices under 1.5G solar illuminations.

The FF has increased for the devices fabricated by TiO₂ electrospun nanofibers on ZnO CBL from 0.51 to 0.53 compared to the devices fabricated by TiO₂ CBL. The improved FF attributed to a better ohmic contact for ZnO (CBL)/electrospun TiO₂ nanofibers based devices compared to other devices [48]. This is evidenced by the decrease in series resistance from 4.28Ω·cm² (TiO₂ (CBL)/electrospun TiO₂ nanofibers) to 1.27Ω·cm² (ZnO (CBL)/electrospun TiO₂ nanofibers).

The PCE of the devices fabricated by ZnO (CBL)/electrospun TiO₂ nanofibers reached to 4.27±0.01%, which is much higher than both of the other devices fabricated with nanofibers and three times higher than the devices fabricated without nanofibers. The major contribution to this increase is by the FF and *V*_{oc}, though *J*_{sc} of all the devices is higher, as metal oxide nanofibers act as a part of the double heterojunction. The introduction of ZnO (CBL) along with TiO₂ electrospun nanofibers facilitate better alignment between the work function of ITO and LUMO of PCBM [18], resulted in an improved PCE.

Table-1: The OPV device parameters under 1.5G solar illuminations.

Device structure	<i>V</i> _{oc} (V)	<i>J</i> _{sc} (mA/cm ²)	FF	PCE (%)
ITO/ZnO/blend/PEDOT: PSS/Ag	0.49	5.56	0.49	1.34±0.02
ITO/TiO ₂ /TiO ₂ nanofibers/blend/PEDOT: PSS/Ag	0.61	12.76	0.51	3.97±0.01
ITO/ZnO/ZnO nanofibers/blend/PEDOT: PSS/Ag	0.61	11.67	0.52	3.70±0.03
ITO/ZnO/TiO ₂ nanofibers/blend/PEDOT: PSS/Ag	0.62	12.98	0.53	4.27±0.01

The IPCE for all the devices is displayed in Fig. 5. The maximum IPCE obtained is 75.27% at 506nm for ZnO (CBL)/ electrospun TiO₂ nanofibers based OPV devices. Contrarily, the IPCE has decreased to 63% for devices fabricated by ZnO (CBL)/ electrospun ZnO nanofibers. The possible reason evidenced by UV-vis absorption (Fig. 3), is the reduced absorption of ZnO nanofibers compared to TiO₂ nanofibers. The increased IPCE in the visible range (450-550nm) is attributed to efficient charge collection and extraction by the electrode. The increase in IPCE, for metal oxide nanofibers based devices is in agreement with the increased J_{sc} , indicating that maximum carriers were collected by nanofibers both from P3HT and PCBM.

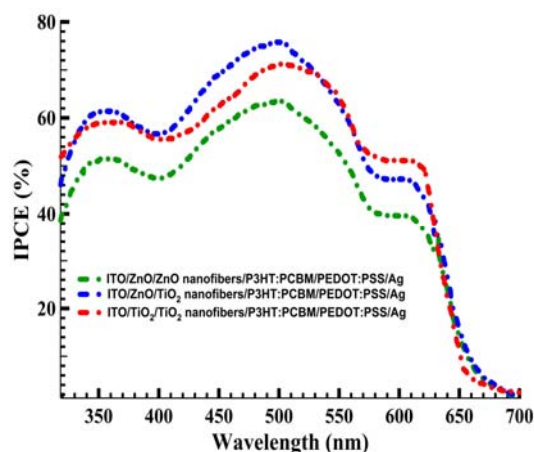


Fig. 5: The incident photon to power conversion efficiency of the fabricated photovoltaic devices.

Experimental

Synthesis of Nanofibers

Electrospun nanofibers were synthesized by optimized precursor sol-gel. The various electrospinning parameters were optimized and kept fixed for both (TiO₂ and ZnO nanofibers) structures and two separate sols for electrospinning were prepared as described below.

TiO₂/poly(vinylpyrrolidone) (PVP) precursor homogenous sol-gel was prepared by mixing a solution of 0.15ml titanium tetraisopropoxide (Ti(OiPr)₄) (Sigma Aldrich) and 0.3g PVP (Sigma Aldrich MW 40, 000) dissolved in 5ml ethanol. The sol was stirred at room temperature for 10h, while 0.25ml acetic acid was added drop wise during the process.

ZnO/PVP sol-gel was obtained by dissolving 0.15g of zinc acetate dehydrate and 0.3g of PVP (MW 40,000) in 3ml of 2-methoxyethanol. 1.5ml of isopropanol along with 0.05ml ethanolamine was added and the mixture was stirred for 14h at room temperature to get homogenous sol for electrospinning.

The precursor mixture was immediately loaded into a plastic syringe equipped with a needle made of stainless steel having an internal diameter of 0.25mm. The distance between the tip of the needle and the collector plate was fixed to 12cm. The nanofibers were collected by the substrate placed on a collector plate by applying an optimum high voltage of 10kV between the needle and the collector plate. The flow rate and electrospinning time was optimized to 0.25ml/h and 10min respectively. The role of humidity and temperature is always related to the diameter and the network layer thickness of the nanofibers, so electrospinning was performed in a low humidity (25~35%) environment at room temperature. The as spun nanofibers were left in the air for more than 12h to allow the complete hydrolysis. Finally, composite nanofibers were calcined in air at 350°C for 3h to obtain a continuous nanofibrous network.

Device Fabrication

Electrospun nanofibers metal oxide based inverted OPV devices were fabricated on an indium doped tin oxide (ITO) (sheet resistance of 17Ω/sq) coated glass substrate. The substrate was first cleaned by sonication for 10min each in detergent, de-ionized water, acetone and isopropanol, and then dried by nitrogen flow. The cathode buffer layer (CBL) (~20nm) of TiO₂ and ZnO was deposited by spin coating respective solution followed by 1h hydrolysis at room temperature and annealing at 200°C. The solution for TiO₂ CBL was synthesized by stirring a mixture of dissolved Ti(OiPr)₄ (1.0ml) in (5ml) 2-MeEtOH and (1ml) MEA, at 80°C for two hours. ZnO CBL was spin coated by a solution of (0.5g) Zinc acetate dehydrate, (5ml) 2-MeEtOH, and (0.15ml) MEA stirred at 60°C for 2h. The metal oxide nanofibers were electrospun on CBL as mentioned above. A blend of poly (3-hexylthiophene) (P3HT) (Rieke Metals, Mw 48000, regioregularity 93%) and PCBM (Ossila) was prepared by mixing a solution of P3HT (12mg/ml) and PCBM (10mg/ml) dissolved in chlorobenzene and spin coated at 1250 RPM for 40s. Then a layer of PEDOT: PSS (Sigma Aldrich) was spin coated at 4000 RPM for 60s. The devices were annealed at 140°C for 10min prior to the deposition of 100nm thick top Ag electrode. In

order to confirm the reproducibility of the results, each of the devices was fabricated and characterized four times under identical conditions. The structures studied in this report are; a) ITO/ZnO (CBL)/blend/PEDOT: PSS/Ag ; b) ITO/TiO₂ (CBL)/TiO₂ nanofibers/ blend/ PEDOT: PSS/Ag; c) ITO/ZnO (CBL)/ZnO nanofibers/blend/PEDOT: PSS/Ag; and d) ITO/ZnO (CBL)/TiO₂ nanofibers/blend/PEDOT: PSS/Ag.

The morphology, diameter, and porosity of the nanofibers were studied by Hitachi S-4700 field emission scanning electron microscope (FE-SEM), and ImageJ software. The thickness of the layers was measured by α -step surface profiler while UV-Vis absorption spectrum was analyzed by Perkin Elmer Lambda 750 spectrophotometer. PV Measurements Inc was used to measure the incident photon to current conversion efficiency (IPCE). The photovoltaic performance of fabricated devices was studied by a solar simulator AM 1.5G, under illumination of 100mW/cm² (Newport 69911). Cell current-voltage characterization was conducted by using Keithley 236 source meter.

Conclusion

ZnO (CBL) reduced the series resistance of the devices when used with TiO₂ electrospun nanofibers compared to the devices fabricated by identical oxide CBL and nanofibers. The double heterojunction provided by electrospun nanofibers has improved the J_{sc} of the OPV devices by collecting and transporting the maximum carriers from P3HT: PCBM to the electrode. The combination of ZnO (CBL) with electrospun TiO₂ nanofibers has improved the PCE up to 4.27% by improving the V_{oc} (0.62V) and FF (0.53) due to broad absorption of light spectrum and reduced series resistance through better ohmic contact.

Acknowledgments

The authors are highly thankful to Higher Education Commission Pakistan, for their financial support to this work. We acknowledge the efforts of Gwangju Institute of Science and Technology, Korea for various characterizations during this work.

References

1. F. C. Krebs, *Polymer Photovoltaics A Practical Approach*, SPIE (2008).
2. R. G. V. N. Espinosa, M. S. García-Cascales and A. Urbina, *International Conference on Renewable Energies and Power Quality (ICREPEQ'10) Granada (Spain)*, 23th to 25th March, 2010 (2010).
3. L. Sangchul, Y. Jun Seok, J. Yongsung, C. Chunhum, K. Dong Yu, N. Seok-In, L. Byoung Hun, L. Takhee, *Nanotechnology*, **23**, 344013 (2012).
4. J. C. Wang, W. T. Weng, M. Y. Tsai, M. K. Lee, S. F. Horng, T. P. Perng, C. C. Kei, C. C. Yu and H. F. Meng, *Journal of Materials Chemistry*, **20**, 862 (2010).
5. E. Bundgaard, O. Hagemann, M. Manceau, M. J. Å, Rgensen and F. C. Krebs, *Macromolecules*, **43**, 8115 (2010).
6. M. M. Voigt, R. C. I. Mackenzie, S. P. King, C. P. Yau, P. Atienzar, J. Dane, P. E. Keivanidis, I. Zadrazil, D. D. C. Bradley and J. Nelson, *Solar Energy Materials and Solar Cells*, **105**, 77 (2012).
7. H. Kidowaki, T. Oku and T. Akiyama, *Fabrication and characterization of CuO/ZnO solar cells*, in, IOP Publishing, 2012, pp. 012022.
8. H. G. Jeon, C. Y. Cho, J. C. Shin and B. Park, *Journal of Materials Chemistry*, **22**, 23022 (2012).
9. Z. Chen, Z. B. Deng, M. Y. Zhou, Z. Y. Lü, H. L. Du, Y. Zou, Y. H. Yin and J. C. Lun, *Chinese Physics Letters*, **29**, 078801 (2012).
10. R. Søndergaard, M. Helgesen, M. Jørgensen, F. C. Krebs, *Advanced Energy Materials*, **1**, 68 (2011).
11. K. X. Steirer, M. O. Reese, B. L. Rupert, N. Kopidakis, D. C. Olson, R. T. Collins and D. S. Ginley, *Solar Energy Materials and Solar Cells*, **93**, 447 (2009).
12. W. R. Saleh, N. M. Saeed, W. A. Twej, M. Alwan, *Advances in Materials Physics and Chemistry*, **2**, 11 (2012).
13. S. Zandi, P. Kameli, H. Salamati, H. Ahmadvand and M. Hakimi, *Physica B: Condensed Matter*, **406**, 3215 (2011).
14. Z. Song, T. A. Kelf, W. H. Sanchez, M. S. Roberts, J. Rička, M. Frenz, A. V. Zvyagin, *Biomedical Optics Express*, **2**, 3321 (2011).
15. J. Ajuria, I. Etxebarria, W. Cambarau, U. Munecas, R. Tena Zaera, J. C. Jimeno and R. Pacios, *Energy and Environmental Science*, **4**, 453 (2011).
16. Y. Sun, J. H. Seo, C. J. Takacs, J. Seifert and A. J. Heeger, *Advanced Materials*, **23**, 1679 (2011).
17. J. You, C. C. Chen, L. Dou, S. Murase, H. S. Duan, S. A. Hawks, T. Xu, H. J. Son, L. Yu, G. Li and Y. Yang, *Advanced Materials*, **24**, 5267 (2012).
18. T. Z. Oo, D. C. R. Panicker, N. Yantara, R. R. Prabhakar, L. H. Wong, N. Mathews and S. G. Mhaisalkar, *Organic Electronics*, **13**, 870 (2012).

19. Y. Matsuo, J. Hatano, T. Kuwabara and K. Takahashi, *Applied Physics Letters*, **100**, 063303 (2012).
20. S. H. Park, A. Roy, S. Beaupré, S. Cho, N. Coates, J. S. Moon, D. Moses, M. Leclerc, K. Lee and A. J. Heeger, *Nature Photonics*, **3**, 297 (2009).
21. A. Roy, S. H. Park, S. Cowan, M. H. Tong, S. Cho, K. Lee and A. J. Heeger, *Applied Physics Letters*, **95**, 013302 (2009).
22. J. H. Park, T. W. Lee, B. D. Chin, D. H. Wang and O. O. Park, *Macromolecular Rapid Communications*, **31**, 2095 (2010).
23. H. Fu, M. Choi, W. Luan, Y. S. Kim, S. T. Tu, *Solid State Electronics*, **69**, 50 (2012).
24. S. Ren, L. Y. Chang, S. K. Lim, J. Zhao, M. Smith, N. Zhao, V. Bulović, M. Bawendi and S. Gradedecak, *Nano Letters*, **11**, 3998 (2011).
25. H. W. Choi, K. S. Lee and T. L. Alford, *Applied Physics Letters*, **101**, 153301 (2012).
26. Y. Zhou, M. Eck, C. Men, F. Rauscher, P. Niyamakom, S. Yilmaz, I. Dumsch, S. Allard, U. Scherf and M. Kräger, *Solar Energy Materials and Solar Cells*, **95**, 3227 (2011).
27. Y. H. Lin, P. C. Yang, J. S. Huang, G. D. Huang, I. J. Wang, W. H. Wu, M. Y. Lin, W. F. Su and C. F. Lin, *Solar Energy Materials and Solar Cells*, **95**, 2511 (2011).
28. G. K. Mor, K. Shankar, M. Paulose, O. K. Varghese and C. A. Grimes, *Applied Physics Letters*, **91**, 152111 (2007).
29. J. Lee and J. Y. Jho, *Solar Energy Materials and Solar Cells*, **95**, 3152 (2011).
30. C. Liu, Z. Chen, H. Wang, S. Jha, W. Zhang, I. Bello and J. Zapfen, *Applied Physics Letters*, **100**, 243102 (2012).
31. M. Tanveer, A. Habib and M. B. Khan, *Materials Science and Engineering: B*, **177**, 1144 (2012).
32. M. C. Akgun, Y. E. Kalay and H. E. Unalan, *Journal of Materials Research*, **1**, 1 (2012).
33. P. V. Kamat, *The Journal of Physical Chemistry C*, **116**, 11849 (2012).
34. L. Francis, A. Sreekumaran Nair, R. Jose, S. Ramakrishna, V. Thavasi and E. Marsano, *Energy*, **36**, 627 (2011).
35. S. H. Park, A. Roy, S. Beaupre, S. Cho, N. Coates, J. S. Moon, D. Moses, M. Leclerc, K. Lee and A. J. Heeger, *Nature Photonics*, **3**, 297 (2009).
36. K. Vakhshouri, S. V. Kesava, D. R. Kozub, E. D. Gomez, *Materials Letters*, **90**, 97 (2013).
37. Y. Wang, W. Wei, X. Liu and Y. Gu, *Solar Energy Materials and Solar Cells*, **98**, 129 (2012).
38. J. J. Zhu, Z. Q. Xu, G. Q. Fan, S. T. Lee, Y. Q. Li and J. X. Tang, *Organic Electronics*, **12**, 2151 (2011).
39. Z. Q. Xu, F. Z. Sun, J. Li, S. T. Lee, Y. Q. Li and J. X. Tang, *Applied Physics Letters*, **99**, 203301 (2011).
40. D. Zhao, S. Tan, L. Ke, P. Liu, A. Kyaw, X. Sun, G. Lo and D. Kwong, *Solar Energy Materials and Solar Cells*, **94**, 985 (2010).
41. D. Rana Bekci and S. Erten Ela, *Renewable Energy*, **43**, 378 (2012).
42. H. P. Kim, H. J. Lee, A. R. b. Mohd Yusoff and J. Jang, *Solar Energy Materials and Solar Cells*, **108**, 38 (2013).
43. Y. J. Kang, C. S. Kim, D. S. You, S. H. Jung, K. Lim, D. G. Kim, J. K. Kim, S. H. Kim, Y. R. Shin, S. H. Kwon and J. W. Kang, *Applied Physics Letters*, **99**, 073308 (2011).
44. T. Kuwabara, H. Sugiyama, M. Kuzuba, T. Yamaguchi and K. Takahashi, *Organic Electronics*, **11**, 1136 (2010).
45. C. Jagdish Bhongale and M. Thelakkat, *Solar Energy Materials and Solar Cells*, **94**, 817 (2010).
46. H. Schmidt, H. Flugge, T. Winkler, T. Bulow, T. Riedl, W. Kowalsky, *Applied Physics Letters*, **94**, 243302 (2009).
47. S. D. Yambem, K. S. Liao, N. J. Alley and S. A. Curran, *Journal of Materials Chemistry*, **22**, 6894 (2012).
48. Y. Jia, L. Yang, W. Qin, S. Yin, F. Zhang and J. Wei, *Renewable Energy*, **50**, 565 (2013).